Journal of Environmental Radioactivity 164 (2016) 26–35

Contents lists available at ScienceDirect

Journal of Environmental Radioactivity

journal homepage: www.elsevier.com/locate/jenvrad

High-resolution radiation mapping to investigate FDNPP derived contaminant migration

P.G. Martin [a, *], O.D. Payton [a], Y. Yamashiki [b], D.A. Richards [c], T.B. Scott [a]

[a] Interface Analysis Centre, HH Wills Physics Laboratory, University of Bristol, Bristol BS8 1TL, UK
[b] Graduate School of Advanced Integrated Studies in Human Survivability, Kyoto University, Kyoto 606-8501, Japan
[c] School of Geographical Sciences, University of Bristol, Bristol BS8 1SS, UK

ARTICLE INFO

Article history:
Received 7 April 2016
Received in revised form
26 May 2016
Accepted 28 June 2016
Available online 7 July 2016

Keywords:
Fukushima
Iitate
Radiation mapping
Fallout
Contamination
Migration

ABSTRACT

As of March 2016, five years will have passed since the earthquake and ensuing tsunami that crippled the Fukushima Daiichi Nuclear Power Plant on Japan's eastern coast, resulting in the explosive release of significant quantities of radioactive material. Over this period, significant time and resource has been expended on both the study of the contamination as well as its remediation from the affected environments. Presented in this work is a high-spatial resolution foot-based radiation mapping study using gamma-spectrometry at a site in the contaminated Iitate Village; conducted at different times, seventeen months apart. The specific site selected for this work was one in which consistent uniform agriculture was observed across its entire extent. From these surveys, obtained from along the main northwest trending line of the fallout plume, it was possible to determine the rate of reduction in the levels of contamination around the site attributable to the natural decay of the radiocesium, remediation efforts or material transport. Results from the work suggest that neither the natural decay of radiocesium nor its downward migration through the soil horizons were responsible for the decline in measured activity levels across the site, with the mobilisation of contaminant species likely adhered to soil particulate and the subsequent fluvial transport responsible for the measurable reduction in activity. This transport of contaminant via fluvial methods has already well studied implications for the input of contaminant material entering the neighbouring Pacific Ocean, as well as the deposition of material along rivers within previously decontaminated areas.

1. Introduction

Following the magnitude 9.0 Great Tōhoku earthquake (Simons et al., 2011) occurred the 15 m high tsunami that was responsible for overtopping the defence walls and crippling the Fukushima Daiichi Nuclear Power Plant (FDNPP) in mid-March 2011. Over the succeeding days as pressures and temperatures rose within the reactor pressure vessel, numerous explosions occurred at the coastal multiple-reactor site, with a total estimated radiation release of 520 (300–800) PBq (Steinhauser et al., 2014), one tenth of the total activity released as a result of the Chernobyl accident in the former USSR twenty-five years earlier (Steinhauser et al., 2014). In comparison, these two International Nuclear Event Scale Level 7 rated events (IAEA, 2012), the amount of refractory elements (including actinide species) released from the Chernobyl accident was about four orders of magnitude greater than that from Fukushima. In Chernobyl the majority of contamination was spread over Russia and central Europe, whereas more than 80% of the activity resulting from Fukushima was transported outwards east into the Pacific Ocean (Buesseler et al., 2011; Masson et al., 2011). From the succession of releases that occurred, it is the medium-lived fission product isotopes of cesium, ^{134}Cs and ^{137}Cs, with half-lives of 2.065 and 30.2 years respectively (CRC Press, 2015) that are the primary source of contamination and hence the subject of the extensive decontamination efforts (Hardie and McKinley, 2014; Japanese Ministry of the Environment, 2013; Miyahara et al., 2012; Yasutaka and Naito, 2015).

Following the release, a series of high altitude aerial surveys (with results corrected to height of 1 m) were conducted using manned aircraft at altitudes between 150 and 700 m, to provide initial results on the spread of the contamination and yielding a spatial resolution of hundreds of square meters per data point

* Corresponding author.
E-mail address: peter.martin@bristol.ac.uk (P.G. Martin).

http://dx.doi.org/10.1016/j.jenvrad.2016.06.025

(MEXT and United States DoE, 2011). Over the succeeding weeks and months, further manned surveys were conducted to increase both the spatial resolution of the results and the area covered – resulting in a contamination map extending across the majority of the country (MEXT, 2013). Resolution was improved still further by the deployment of unmanned helicopters (Sanada et al., 2014, 2012), used widely within Japan for agricultural crop-spraying. Operating at reduced altitudes (typically around 80 m), these systems considerably increased the achievable resolution to the order of 25 m per pixel. As well as markedly increasing the resolution, the deployment of unmanned systems has the greater additional benefit of not exposing those conducting the survey to potentially significant levels of radiation, with those performing the survey able to conduct the work from radiologically safe locations. Yet further improvement on resolution was brought about by the use of multi-rotor unmanned aerial vehicle (UAV) platforms to record contamination at the meter scale (MacFarlane et al., 2014; Martin et al., 2016, 2015). Unlike the larger unmanned helicopters which consist of a single centre-mounted propeller, multi-rotors are comprised of multiple (typically between 4 and 8) smaller motors and propellers constituting a smaller, more lightweight and manoeuvrable airframe. Through the use of such lightweight systems, a resolution comparable to foot-based surveying is achieved, also with the benefit of eliminating exposure to those conducting the work and improving detector sensitivity by removing a significant attenuating mass (the human surveyor) (Buchanan et al., 2016). It is this high-resolution radiation mapping that is central to the complete and efficient remediation of the large contaminated region of Japan surrounding the Fukushima Plant.

In addition to the work undertaken to accurately map and quantify the extent of the radionuclide contamination, determination of the physical behaviour of this released material within the environment has also been the subject of extensive study. The analysis of the vertical depth profiles of ^{134}Cs and ^{137}Cs have been made by multiple authors since the events in Japan, across numerous types of localities around Fukushima Prefecture (Kato et al., 2012; Kinoshita et al., 2011; Koarashi et al., 2012; Ohno et al., 2012; Stohl et al., 2012; Tagami et al., 2011; Teramage et al., 2014; Yasunari et al., 2011) with the vast majority of the total cesium inventory within the soil existing within the very upmost portion of the column. In early results on bare soil exposures by both Kato et al. (2012) and Ohno et al. (2012) over 90% of radiocesium contamination was observed, via soil coring, to exist within the top 4 cm. Subsequent work by Teramage et al. (2014) on vegetated land contaminated by the release events, found that 52% and 47% of the ^{134}Cs and ^{137}Cs inventories respectively existed within the raw organic layer (litter and fermented layers), with correspondingly less inventory existing as part of the underlying soil – concentrated still in the underlying uppermost soil layers.

Studies prior to Fukushima, as a result of the Chernobyl accident, focused on the interaction of cesium ions within a soil; concluding that inner-sphere complexes onto high surface-area clays such as illite, montmorillonite and vermiculite were responsible for their fixation and immobilisation (Sawhney, 1972). Staunton et al. (2002) examined the role of organic matter in the behaviour of environmental cesium, concluding that a greater fraction of organics as part of a soil contributes to a reduction in cesium absorbed onto clays; with organic matter allowing for plants to uptake the radionuclide that would otherwise sorb onto clays. Comparative work following the FDNPP release concluded that cesium retention was similarly attributable to fixation onto clay-type minerals with a similar influence imparted by organic material (Kamei-Ishikawa et al., 2008; Kogure et al., 2012; Qin et al., 2012). Recent work by Mukai et al. (2016) studying specific clay minerals from around Fukushima Prefecture observed that partially-vermiculitized biotite (termed "weathered biotite") sorbed markedly more ^{137}Cs that any of the other clay species such as illite, smectite, kaolinite or allophane. Kaneko et al. (2015) quantified that clays, mica, vermiculite, chlorite and smectite were responsible for adsorbing more than 70% of the total Cs in the soil profile, with additional aggregation of these sub-micron particles further limiting movement within the soil profile. Kaneko et al. also comment that these larger particles could potentially be transported as suspended colloids, although which should be considered when predicting future migration.

In the previously highlighted work by Kato et al. (2012) conducted at a site 6.0 km NW of the site examined here, analysis of soil core samples in an area exhibiting a slightly reduced level of contamination and comparable cultivation were examined. The soil in this work, defined as a silty sandy loam, was composed predominantly of silt and sand with lesser clay and gravel constituents. Similar works by Lepage et al. (2015) also performed soil and depth distribution analysis at a location (point P10) within close proximity to the site of this work, along rivers of the Nitta River catchment. Analysis of the soil determined an elevated total organic content over other sites within the catchment as well as a higher clay content (although a different, larger, defining diameter was employed). Despite this observed variation in pedology across the region surrounding the Iitate study site, the careful selection of this site over others, with respect to parameters discussed subsequently (including the existence of organic rich horizons, differing irrigation methods and the application of fertilisers to the site) allows for these effects to be excluded.

2. Experimental

2.1. Survey site

The area chosen for this study was a series of adjoining fields located in southern Iitate Village (37°36′52.1″ N, 140°42′30.2″ E), Fukushima Prefecture. Within the 100 × 130 m site, dissected by both a tarmacked road and a small NW-SE trending stream (flowing eastwards eventually into the Pacific Ocean, north of Minamisoma), numerous different land uses/crop types were observed to exist. Results of aerial monitoring by MEXT (2011) quantified the dose-rate at between 9.5 and 19.0 μSv/hr immediately following the release, with survey meter readings confirming the dose-rate 8 weeks later, in June 2011, at 10 μSv/hr (NRA, 2011). This site exists within close proximity to a number of existing JAEA test sites, between three and six km away in the neighbouring Kawamata area. These important sites were established to examine the changing distributions of contaminant species over the years succeeding the radioactive release. As is consistent with numerous settlements around the Fukushima Prefecture, this study area is located within an east-west trending valley floor ~500 m in width, at an elevation of 600 m OD, with inclined 200 m high valley sides running parallel to the north and south of the site. From the coastal plains bordering the Pacific Ocean where the FDNPP is located; composed of geologically young Tertiary and Quaternary sedimentary rocks, the mountainous plateaus to the west constitute a wider range of lithologies, including Cretaceous intrusive igneous rocks, regional metamorphic rock units and a suite of sedimentary lithologies – separated via numerous fault systems (Geological Survey of Japan, 2015).

Located within what is defined as 'Area 2', close to the border with 'Area 3', Fig. 1. (as of September 5th, 2015), this site is classified as an area "in which residents are not permitted to live" (with Area 3 representing regions where it is "expected that the residents will have difficulties in returning for a long time") due to the considerable levels of radiation (METI, 2015).

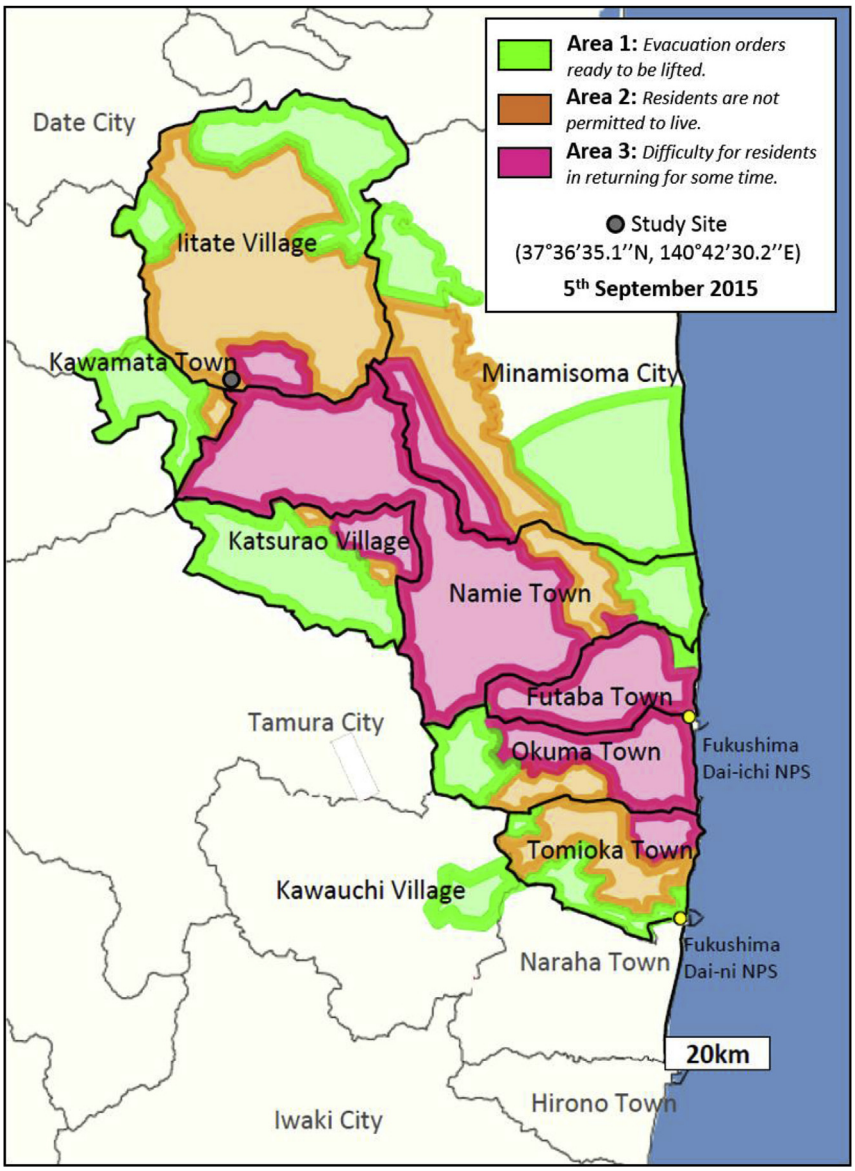

Fig. 1. Areas to which Evacuation orders have been issued (as of 5th September 2015), with the location of the study site on the Kawamata Town – Iitate Village border identified. Modified from METI (2015).

At the time of the initial radiological survey in May 2014, no remediation had commenced at the site; with the initiation of clean-up works on portions of the site occurring shortly before the second survey in October 2015. This work included the clearance of plant and crop material from fields, as well as the removal of the top 10–15 cm of soil, with clean soil eventually being replaced onto the site. Additional measures included the pressure washing and scrubbing of hard surfaces such as rocks and roads as well as the stripping and deep-cleaning of trees.

2.2. Radiological mapping

In order to produce the greatest precision map of the distribution of contaminants, foot-based mapping was conducted. The lightweight radiation mapping system deployed previously via unmanned aerial vehicle (UAV) described within MacFarlane et al. (2014) and Martin et al. (2016) was carried in a backpack by the operator. A detailed description of the system is described in these works, consisting of a lightweight gamma-ray detector, an environmentally sealed processing unit along with a rugged external GPS unit. Combined, the entire system has a mass of 260 g (60 g detector/200 g electronics). The uncollimated coplanar-grid GR1 detector by Kromek™ (Co. Durham, UK) has an energy range of 30 keV to 3.0 MeV with a maximum count rate of 30,000 counts per second (CPS) and energy resolution of <2.5% Full Width at Half Maximum (FWHM) at 662 keV over the detectors 4096 channels. Electrical noise within the detector was <10 keV FWHM. The 10 × 10 × 10 mm Cadmium Zinc Telluride (CZT) crystal is enclosed within a 25 × 25 × 63 mm aluminium case (Kromek Group PLC, 2015).

Control of the detector was performed by an Arduino Mega ADK microcontroller (Scarmagno, Italy). Data from the gamma-spectrometer was sampled at 2 Hz as a series of gamma energies incident onto the detector during the preceding 0.5 s. The location at which radiation was measured was obtained through the use of an Adafruit Ultimate GPS breakout board installed within the setup,

this chip could acquire position accurate to approximately 0.5 m. An external GPS aerial, which was affixed to the outside of the backpack, was attached to this board to provide enhanced GPS reception. Data collected was written in real-time to an on-board micro-SD card as well as being transmitted in near real time [500 ms delay] via an encrypted radio frequency data stream back to a remote base station where progress and coverage could be monitored.

For ease as well as consistency with standard radiological surveys; all of which are normalised to a height of 1 m above the ground surface, the detection system was maintained in the backpack 1 m above the ground surface pointing vertically down. To conduct the surveys, a back and forth "zig-zag" grid pattern was employed across the survey site, with the operator maintaining a consistent 1 m separation between transects wherever practical (slopes and ditches across parts of the site made minor deviations unavoidable). A slow walking pace of approximately 3.5 km/h (1 m/s) (calibrated against a known transect distance) was preserved to ensure the greatest achievable resolution (greatest number of sampling points over an area).

Previous work by Malins et al. (2015) within the Nakadori area of eastern Japan, west of the FDNPP, assessed the influence of topography on measured radiation levels at differing survey altitudes as well as at ground level. It was shown in this work that in high-altitude surveys performed at heights of 300 m above ground level, topography can introduce a change up to 50% in air dose-rate compared to if the ground below were uniformly flat. However, Malins et al. (2015) ultimately conclude that the effects of topography on dose-rate are minimal, as heterogeneity in the source represents a more significant factor in variation of local air dose-rate at altitude, with the impact of topography on low-altitude and ground surveys being negligible. As the gamma half-distance for ^{137}Cs is on the order of 70 m (obtained via the mass attenuation coefficient of "air" at the characteristic 662 keV gamma energy) and with the survey site was greater than 150 m from each of the valley sides, the influence of the surrounding valley topography on results obtained during this work are hence considered negligible. Hence, the effects of attenuation on gamma-rays via the 1 m portion of air present between the source and detector during this work is also considered to be negligible.

In order to directly correlate dose-rate (μSv/hr) with measured CPS values, a series of both in-lab and field-based calibration exercises were conducted. Prior to fieldwork, both the gamma-spectrometer used and a portable dosimeter from RADEX™ (Moscow, Russia) were exposed to a series of cesium calibration sources; with the corresponding dose-rate given by the dosimeter and count-rate from the gamma-spectrometer in each instance recorded. Whilst in the field, a number of dosimeter readings from the RADEX™ unit were obtained by the operator at known localities, and directly compared with values produced by the gamma-spectrometer system at these same points. The graph shown in Fig. 2 highlights the strongly-linear relationship between these two values.

To assess the influences of slight topological variations within the contamination affected region (e.g. surrounding buildings, presence of neighbouring trees and local-scale topography) on dose-rate and CPS, both measurements (as described above) were taken additionally at other sites in Fukushima Prefecture (Site B – Namie Town (37°33′55.9″ N, 140°44′37.7″ E) and Site C – Katsurao Village (37°30′27.2″ N, 140°49′54.5″ E)). As is shown also within Fig. 2, a good agreement with the study site, the topic of the work presented in this text (Site A – Iitate Village), is witnessed for these additional sites. Site B – Namie Town and Site C – Katsurao Village feature marked local variations in their topography as well as neighbouring buildings and trees which could present a

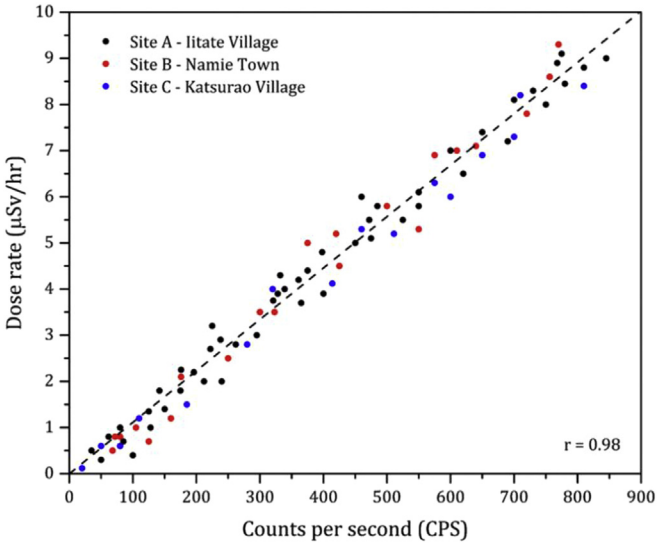

Fig. 2. Dose rate (μSv/hr) vs. counts per second (CPS) calibration for the detection system performed at the study site (Site A – Iitate Village) as well as two other nearby contamination affected locations (Site B – Namie Town and Site C – Katsurao Village).

contribution to the detected dose. However, the limited degree of spread of each sites data points within Fig. 2 would suggest, as akin the conclusions of Malins et al. (2015), that the effects of any local topography and surrounding structures are minimal and can ultimately be ignored, with source heterogeneity representing the greatest factor to impact the local dose-rate.

Unlike low-altitude airborne systems previously employed by the authors in Japan, where there is no attenuation of gamma-ray photons by the operator to influence results, a marked reduction in measured intensity is introduced using foot-based operations. Early work by Jones and Cunningham (1983) estimated these loses at about 30%, with recent work by Buchanan et al. (2016) on a standard reference human, quantifying count-rate losses for the radiocesium full energy peaks similarly at 20–30%. To maintain consistency, both surveys reported in this work were undertaken by the same operator with an identical survey and system setup.

2.3. Decay-only modelling

To assess the contamination at the site, as well as to quantify previous and predicted future levels, both forward and backwards modelling were conducted. Both of these extrapolations were based on the results of the mapping work performed during May 2014. Only the species ^{134}Cs and ^{137}Cs were used as the contributors to radioactivity in these calculations.

At the time of the material release on 11th March 2011, the activity ratio of ^{134}Cs–^{137}Cs (^{134}Cs/^{137}Cs) was 1:1 (Buesseler et al., 2012; Masson et al., 2011; Merz et al., 2013), with equal proportions of both isotopes, however, the difference in the half-lives of both ^{134}Cs and ^{137}Cs (28 years) leads to the rapid reduction of this ratio over time – due to the decay of ^{134}Cs. To factor for this ever-evolving ratio on the species contributing to detected contamination, the standard equation for the backwards calculation of radioactivity levels in March 2011 comprised a weighting factor from both ^{134}Cs and ^{137}Cs *(Eq. (1))*, where λ represents the decay constant (yr^{-1}) for both cesium species, N_0, the activity at the initial time (March 2011) and N, the activity at time, t (May 2014).

$$N_{0\ (Cs134+Cs137)} = \frac{N_t{}^{(Cs134)}}{e^{-\lambda^{(Cs134)}\times t}} + \frac{N_t{}^{(Cs137)}}{e^{-\lambda^{(Cs137)}\times t}} \quad (1)$$

From measurements of May 2014, forward modelling to estimate future contamination (herein referred to as 'calculated') also featured a weighting factor for both isotopes of cesium (Eq. (2)).

$$N_{t\ (Cs134+Cs137)} = N_{0\ (Cs134)} e^{-\lambda(Cs134)\times t} + N_{0(Cs137)} e^{-\lambda(Cs137)\times t} \quad (2)$$

The values from both forward and back modelling provide baseline values that represent the levels of contamination that would exist across the site at various time periods should a reduction only exist as a function of the natural radioactive decay of the cesium isotopes.

2.4. Depth attenuation modelling

As invoked by Malins et al. (2016), the main mechanism for the decrement of the measured air dose-rate 1 m above the ground surface, in addition to radioactive decay of the species, is the downward migration of cesium into the soil. To assess this factor on the levels of radiation recorded around the site, a mass attenuation coefficient was applied to radiocesium dispersed at various depths throughout the soil profile as described in various scenarios by Kato et al. (2012), Ohno et al. (2012) and Teramage et al. (2014) (Fig. 3). For this simulation, the values for the mass attenuation coefficient for cesium gamma energies were derived from the National Institute of Standards and Technology (NIST) (Hubbell and Seltzer, 2004) database for the constituents (sand, silt and clay) of a typical soil observed within Fukushima, defined by Teramage et al., 2014. The equation used (Eqs. 3 & 4), calculated the radiation intensity that should be measured assuming losses from both radioactive decay and depth attenuation on values calculated from the forward modelling of measured May 2014 data.

$$Intensity = Date\ Calculated\ Value \times Depth\ Attenuation\ Factor \quad (3)$$

$$Intensity = Date\ Calculated\ Value \times exp^{-((\Delta_1[\mu_1\times x_1\times\rho_1])+(\Delta_2[\mu_2\times x_2\times\rho_2])+(\ldots)} \quad (4)$$

where Δ represents the percentage component of cesium at a depth, x (cm), μ, the linear attenuation coefficient (cm^{-1}) for the soil material at that depth and ρ the density (g/cm3) of the soil also calculated at that depth (x). The 'date calculated value' is that produced previously via *Eq. (2)* for the time (t) specified.

3. Results & discussion

3.1. Radiological mapping

The results of the ground-based radiation mapping undertaken during both May 2014 and October 2015 are presented within Figs. 4 and 5 Apparent within Figs. 4 (a) and 5 (a), taken in May 2014, are the high levels of radiation (averaging 398 CPS or 4.8 μSv/hr) distributed across the majority of the site 38 months after the incident. Through the centre of the site, corresponding to the position of the bend in the tarmac road, there is a reduction of 40% on these values, with radiation levels of 2.9 μSv/hr. As no remediation actions had been performed prior to this initial survey, this reduction is ascribed to multiple potential factors including; contaminant material being blown from the exposed road surfaces, removal via adhesion to the tyres of the few vehicles travelling through the area as well as the wash-off onto the land immediately bordering the road due to the high annual precipitation (1130 mm/yr) recorded on Japans main Honshu Island (Japan Meteorological Agency). The greatest contaminant levels on the site were observed in the southern-most field, where a dose-rate of 5.8 μSv/hr was recorded. Unlike the fields to the north, at 4.4 μSv/hr.

The second phase of contamination monitoring during October 2015, shown in Figs. 4 (b) and 5 (b), illustrates a largely similar distribution of radioactivity to the earlier monitoring of May 2014 (Figs. 4 (a) and 5 (a)) with site-wide average dose and count rates of 3.0 μSv/hr and 267 CPS respectively. Like the former mapping work, the northern field exhibits a lower total activity than the site average (222 CPS or 2.7 μSv/hr) with the southern field displaying greater than average radiation levels (351 CPS or 3.9 μSv/hr). As part of the remediation efforts that were occurring at the site during October 2015 under national guidelines (Japanese Ministry of the Environment, 2013), the upper soil layers from the northern portion of the site were being removed and transported for off-site storage. Further to material removal, continual road sweeping and high-pressure scrubbing was performed to remove any radioactivity that became deposited onto surfaces as a result of the nearby clean-up.

3.2. Contamination modelling

Using data obtained from across all the 6300 recorded survey points on the Iitate site (Fig. 4) - during the May 2014 survey, a model predicting both the initial (March 2011) and subsequent levels of radioactivity on the site was constructed. In order to graphically represent a smaller number of illustrative data points (n = 14) with characteristic values from the site-wide survey, a reduced number of points (identified in Fig. 4(a)) were arbitrarily selected (full data presented in Fig. S1). From an average value of 398 CPS (4.8 μSv/hr) recorded in May 2014, calculations place the total activity at the site immediately after the release of material at 770 CPS (9.1 μSv/hr) (Fig. 6), broadly consistent with the value recorded by NRA (NRA, 2011) in the aftermath of the accident. Forward modelling of the contamination levels to October 2015 produces a smaller data range, with a mean value of 323 CPS (3.4 μSv/hr), a total activity reduction of 33%.

Apparent within Fig. 6 (inset) is the spread of measured data; far greater than for values calculated from forward modelling of the May 2014 data. A total range of 310 CPS is evident from the data recorded in October 2015, whereas a difference of only 139 CPS is observed between maximum and minimum values within the calculated data. These differences between values of expected activity verses those measured during the site survey conducted in October 2015 for the 14 representative points are shown within Table 1. The effects of remediation work are evident at several localities; both on the road surface (1, 2 and 3) as well as in fields to the north of the small stream that transects the site (9, 11 and 12) - where the measured value for the activity falls below that of the value proposed to exist in October 2015. Conversely, an increase in the dose-rate and activity is apparent at point 10, where material collected locally from the land surface was bagged and stored within a number of 1 m^3 black storage bags before ultimately being transported offsite to permanent facilities, currently under planning.

At each of the additional points within the site; 7, 8, 13 and 14 – existing to the south of the river on the western and eastern side of the road respectively as well as 5 and 6 - found within the southernmost field, the calculated activity was greater than that actually measured across the site during the October 2015 survey. Typical percentage reductions recorded for remediated areas (e.g. points 9, 11 and 12) were up to nearly 3 times those recorded where no action had occurred (points 6, 13 and 14) (Fig. 7). The activity both

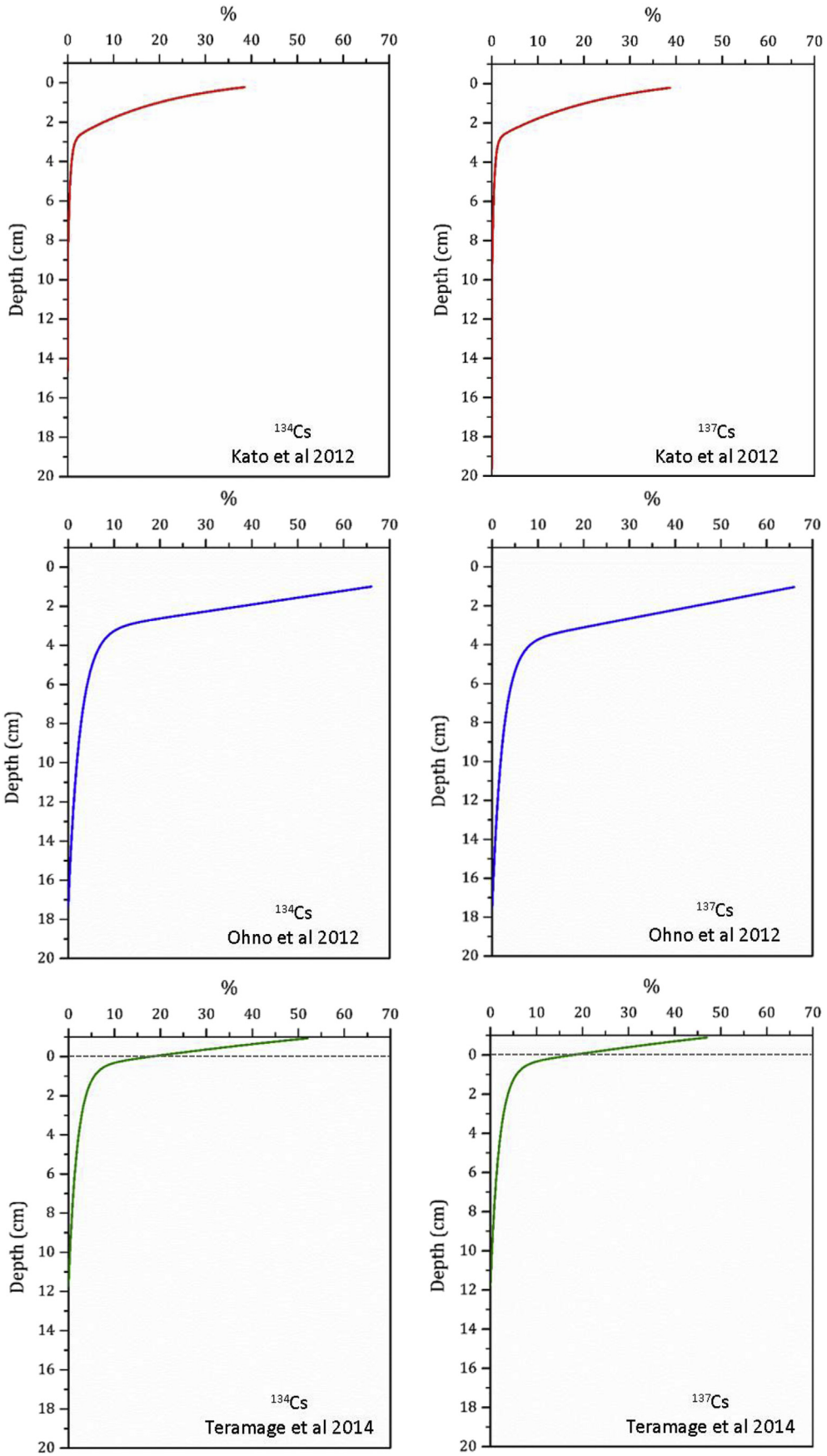

Fig. 3. Soil depth profiles for cesium isotopes ^{134}Cs and ^{137}Cs, modified from previous studies undertaken by Kato et al., 2012, Ohno et al., 2012 and Teramage et al., 2014.

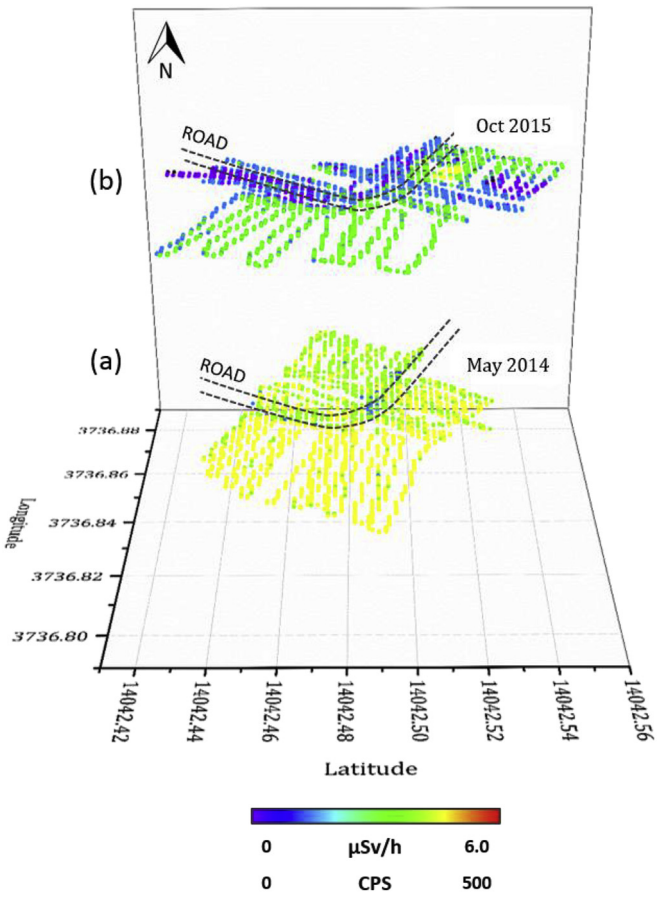

Fig. 4. Offset radiation intensity plots produced from (a) May 2014 and (b) October 2015, with the location of the transecting road identified.

recorded and calculated at point 4 was shown to be nearly-identical, with measured values close to those calculated to have occurred through natural radioactive decay.

3.3. Depth attenuation modelling

As a method to explain the reduction in measured activity (the disparity in values measured and calculated to occur); the influence of downwards cesium migration and attenuation, as proposed by

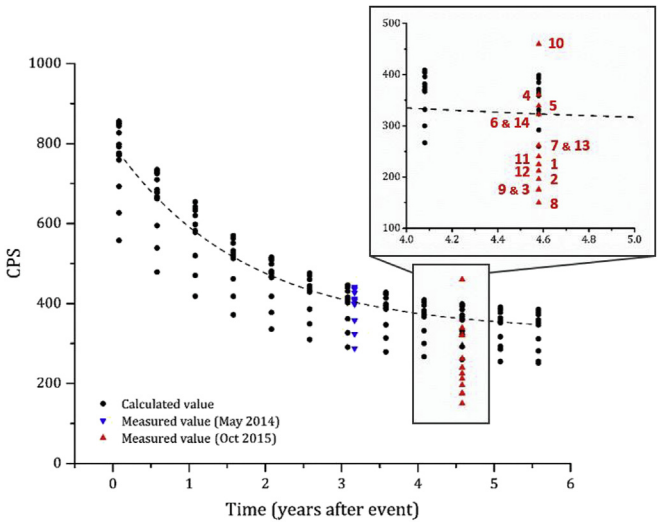

Fig. 6. Calculated and measured activity values from sites across the study area. Site location numbers (1–14) are shown.

Malins et al. (2016), was modelled. The influence of attenuation was investigated on points 5–8 as well as 13 and 14; where the reduction could not be attributed to site clearance.

Results of depth attenuation modelling using vertical cesium concentration profiles from the three different studies, applied to the previously calculated results, are shown within Fig. 8. For each of the sites, both the measured and calculated values are shown in addition to values obtained by applying this attenuation. Percentage attenuations for each model are shown in Table 2, with a reduction in calculated values of between 10.9 and 15.5%. For both points 5 and 6, the application of an attenuation factor to the calculated values yields results that are comparable to those obtained from survey measurements at these points, suggesting that some limited vertical movement of the radioactive material had occurred. However, for points 7 and 8, both located within the portion of land with the river to the north and road to the south, the decrease in activity on the calculated values due to attenuation is not sufficient to reduce levels to those measured during the October 2015 work. As with points 5 and 6, both points 13 and 14, show comparable activities when attenuation corrected calculated values are compared with those measured during the second survey at these points.

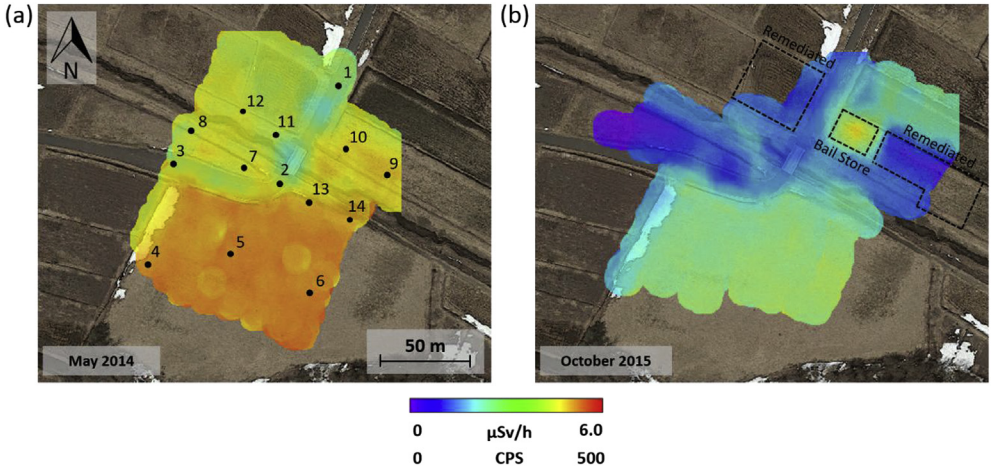

Fig. 5. Radiation intensity maps produced in (a) May 2014 and (b) October 2015, with the location of selected points (1–14) shown.

Table 1
Summary of the differences between calculated and measured values for October 2015 with percentage difference between the two.

Loc. no.	Calculated Oct 2015		Measured Oct 2015		Percentage difference	Notes
	CPS	μSv/hr	CPS	μSv/hr		
1	290	3.2	225	2.6	−30	Road surface; radiation reduction due to cleaning.
2	233	2.6	196	2.1	−25	Road surface; radiation reduction due to cleaning.
3	262	2.9	176	1.9	−40	Road surface; radiation reduction due to cleaning.
4	329	3.8	361	3.9	−2	
5	358	3.9	339	3.8	−15	
6	353	3.9	332	3.7	−18	
7	355	3.9	262	2.9	−34	
8	324	3.7	150	1.6	−58	
9	334	3.8	175	1.9	−53	Remediated land; radiation reduction due to cleaning.
10[a]	331	3.8	460	5.0	25	Bail storage site; increased activity.
11	346	3.9	240	2.7	−38	Remediated land; radiation reduction due to cleaning.
12	322	3.7	212	2.3	−41	Remediated land; radiation reduction due to cleaning.
13	325	3.7	295	3.2	−18	
14	356	3.9	321	3.6	−19	

[a] Location of contaminated material bail store – excluded from average calculation.

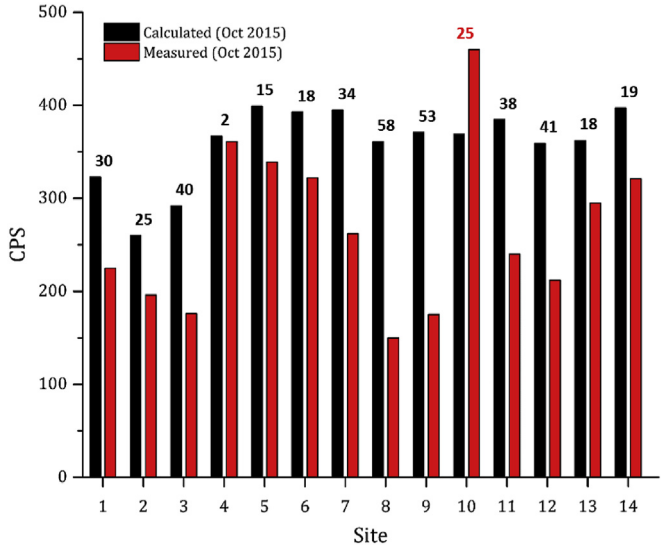

Fig. 7. Comparison of both measured and calculated readings from across the 14 selected sites for October 2015. The percentage difference between the two values is shown.

The marked reduction in the measured activity recorded at points 7 and 8, greater than that attributable to burial-related attenuation and radioactive decay. It is likely attributable to the location at which these points exist - in close proximity to the river; with continual substance input via material erosion and fluvial transport away since the release event. Both points 7 and 8 occur 9 and 13 m away from the small river (1.5 m wide) respectively, which is itself located down a 2.0 m channel. With the survey instrument being maintained in such close proximity to the ground, coupled with the small size of the water body, no effects from water attenuation are hence anticipated. It is this deposition of contaminant species within the affected areas and its subsequent absorption onto fine-scale material, followed by soil erosion associated with frequent extreme typhoon conditions (Japan Meteorological Agency) together with overland flow and run-off that has been invoked and determined by many as responsible for the input of contaminant particulate into the fluvial transport system for eventual transport into the Pacific Ocean (Chartin et al., 2013; Evrard et al., 2013; Nagao et al., 2013; Ueda et al., 2013; Yamashiki et al., 2014).

The site chosen for this work was specifically selected in order to focus on the mechanisms responsible for the measured reduction in dose-rate. Before the 2011 incident, the field on the site existed as

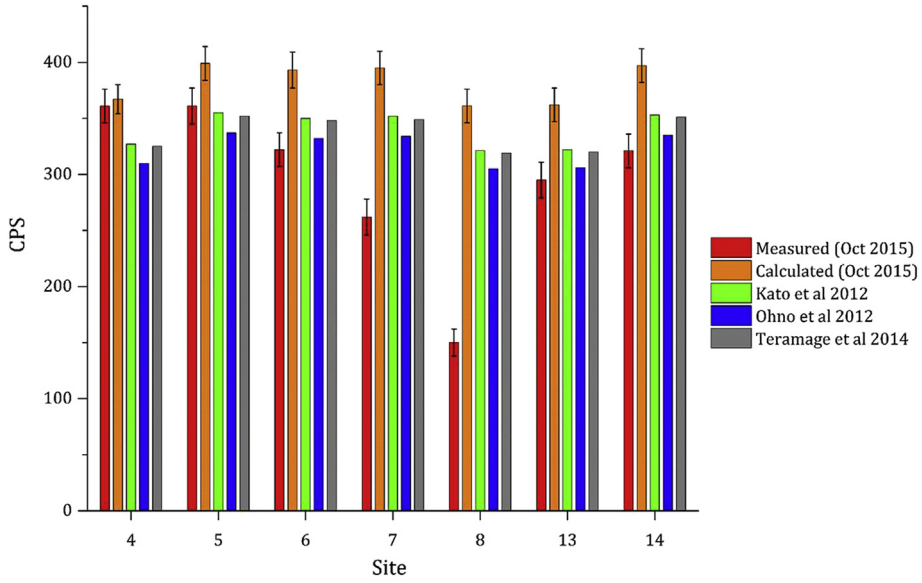

Fig. 8. Influence of vertical cesium infiltration within the soil profile on the attenuation of predicted survey intensity values.

Table 2
Average calculated counts per second (CPS) percentage reduction due to gamma-ray attenuation.

Model	Average percentage Attenuation reduction
T. Ohno et al. (2012)	15.5
H. Kato et al. (2012)	10.9
M. Teramage et al. (2014)	11.6

identical agricultural fields, utilised for the production of the same crop-type by the land-owner (personal communication) it has subsequently regrown since the release. Existing under the same owner, the effects of differences in fertiliser application across the site, which could be invoked as a potential mechanism for differences in the depth of infiltration (due to preferential absorption onto clay mineral surfaces of competing ions such as potassium and sodium over cesium ions) can be disregarded. Similarly, the occurrence of organic-rich horizons which could also serve to influence the downwards penetration of cesium can likewise be omitted for consideration at this site due to the evidence of ploughing having been performed. Typical ploughing by normal agricultural machinery homogenises the uppermost 45 cm of material, and would hence over time eliminate any such heterogeneities. This homogenisation of the soil, overturning the soil profile to bury the surface radioactive material has been employed as a potential method with which to reduce measured air dose-rates within Fukushima (IAEA, 2011; Miyahara et al., 2012), with a reduction factor of 2.3 achieved via this method. To the authors knowledge the site has not been ploughed or worked since the FDNPP incident and ensuing evacuation of the area.

4. Conclusions

This study has utilised radiation mapping within a site in Iitate Village (Fukushima Prefecture) to examine the time resolved behaviour of the contamination deposited as a result of the 2011 FDNPP accident. Using values from site-wide mapping obtained during May 2014, the initial activity at the site immediately after the release was calculated and found to directly compare to levels measured by the monitoring body (NRA). Subsequent forward modelling of the radiation levels also from this point provided calculated levels of the expected contamination. When comparing these calculated levels to those measured during a second survey undertaken 17 months later (October 2015), a wide disparity between both the calculated and measured values was observed.

For those points on the site where the reduction in measured activity, in addition to natural decay, was not influenced by remediation actions or the storage of contaminant material within the site, the effects of downward species migration and associated attenuation were examined. Using this method, the apparent differences between the calculated activity levels and those measured in October 2015 were resolved for a number of points in the survey. Therefore, this excess reduction in radioactivity can likely be attributed to two phenomena. First the attenuation of radiation emitted from fallout particles due to its increasing depth of burial; the radioactive material is slowly migrating downwards. Secondly, for selected points across the survey, such as those close to the river transecting the site, where the influence of vertical attenuation could not reduce the calculated levels to those measured during the October 2015 survey – some other factor in reducing residual radioactivity was in play. Due to their proximity to the river, coupled with the monsoon climate in the region we ascribe wash-off, soil erosion and transportation as the likely mechanisms by which the contamination has been reduced.

Due to this downward migration of radiocesium, the removal of the uppermost soil layers during remediation activities must be sufficient to remove all of the contaminant species vertically dispersed in the soil horizon – therefore remediation should ideally seek to remove soil rather than overturning the top soil layers. The effects of soil material vertical infiltration is seen as strongly contributing to the reduction in measured radiation intensity. As identified within this work, the movement of contaminant material back onto areas previously decontaminated must be considered when undertaking large-scale remediation programmes.

The apparent reduction in activity at certain points over the site, caused by the movement of contaminant containing material into the dissecting river is consistent with the known carriage of radioactive material outwards into the nearby Pacific Ocean via the extensive regional river network – primarily the Abukuma River.

Acknowledgements

The authors wish to thank Sellafield Ltd, UK AWE, Kromek Ltd and the EPSRC for supporting fieldwork within Japan. This work was carried out with support of the University of Bristol and University of Kyoto strategic alliance. Impact Acceleration funding for the development of the system was provided by the EPSRC (Grant Reference: EP/K503824/1). Additional thanks are extended to the two anonymous reviewers whose comments greatly enhanced the quality of the manuscript.

Appendix A. Supplementary data

Supplementary data related to this article can be found at http://dx.doi.org/10.1016/j.jenvrad.2016.06.025.

References

Buchanan, E., Cresswell, A.J., Seitz, B., Sanderson, D.C.W., 2016. Operator related attenuation effects in radiometric surveys. Radiat. Meas. 86, 24–31. http://dx.doi.org/10.1016/j.radmeas.2015.12.029.

Buesseler, K., Aoyama, M., Fukasawa, M., 2011. Impacts of the Fukushima nuclear power plants on marine radioactivity. Environ. Sci. Technol. 45, 9931–9935. http://dx.doi.org/10.1021/es202816c.

Buesseler, K.O., Jayne, S.R., Fisher, N.S., Rypina, I.I., Baumann, H., Baumann, Z., Breier, C.F., Douglass, E.M., George, J., Macdonald, A.M., Miyamoto, H., Nishikawa, J., Pike, S.M., Yoshida, S., 2012. Fukushima-derived radionuclides in the ocean and biota off Japan. Proc. Natl. Acad. Sci. U. S. A. 109, 5984–5988. http://dx.doi.org/10.1073/pnas.1120794109.

Chartin, C., Evrard, O., Onda, Y., Patin, J., Lefèvre, I., Ottlé, C., Ayrault, S., Lepage, H., Bonté, P., 2013. Tracking the early dispersion of contaminated sediment along rivers draining the Fukushima radioactive pollution plume. Anthropocene 1, 23–34. http://dx.doi.org/10.1016/j.ancene.2013.07.001.

CRC Press, 2015. CRC Handbook of Chemistry and Physics - Table of Isotopes, 96th ed (Boca Raton, Florida).

Evrard, O., Chartin, C., Onda, Y., Patin, J., Lepage, H., Lefèvre, I., Ayrault, S., Ottlé, C., Bonté, P., 2013. Evolution of radioactive dose rates in fresh sediment deposits along coastal rivers draining Fukushima contamination plume. Sci. Rep. 3, 3079. http://dx.doi.org/10.1038/srep03079.

Geological Survey of Japan, 2015. Geological Survey of Japan (GSJ). AIST.

Hardie, S.M.L., McKinley, I.G., 2014. Fukushima remediation: status and overview of future plans. J. Environ. Radioact. 133, 75–85. http://dx.doi.org/10.1016/j.jenvrad.2013.08.002.

Hubbell, J.H., Seltzer, S.M., 2004. Tables of X-Ray Mass Attenuation Coefficients and Mass Energy-absorption Coefficients. National Institute of Standards and Technology. Gaithersburg, MD., (Version 1. ed.

IAEA, 2011. Report of the International Mission on Remediation of Large Contaminated Areas Off-site the Fukushima Dai-ichi NPP. IAEA NE/NEF FW/2011.

IAEA, 2012. Re-evaluation of INES Rating; Effect to the Nuclear Facilities from the Earthquake on East Area of Japan. NEWS: The Information Channel on Nuclear and Radiological Events, Vienna.

n.d Japan Meteorological Agency, 2016. Monthly Total of Precipitation (mm) - Japan Meteorological Agency [WWW Document]. http://www.data.jma.go.jp/obd/stats/etrn/view/monthly_s3_en.php?block_no=47401&view=13 (accessed

1.14.16).
Japanese Ministry of the Environment, 2013. Decontamination Guidelines, second ed.
Jones, H.E., Cunningham, J.R., 1983. Physics of Radiology, fourth ed. Thomas Publishing, Springfield, Illinois, USA.
Kamei-Ishikawa, N., Uchida, S., Tagami, K., 2008. Distribution coefficients for 85Sr and 137Cs in Japanese agricultural soils and their correlations with soil properties. J. Radioanal. Nucl. Chem. 277, 433–439. http://dx.doi.org/10.1007/s10967-007-7125-z.
Kaneko, M., Iwata, H., Shiotsu, H., Masaki, S., Kawamoto, Y., Yamasaki, S., Nakamatsu, Y., Imoto, J., Furuki, G., Ochiai, A., Nanba, K., Ohnuki, T., Ewing, R.C., Utsunomiya, S., 2015. Radioactive Cs in the severely contaminated soils near the Fukushima Daiichi nuclear power plant. Front. Energy Res. 3 http://dx.doi.org/10.3389/fenrg.2015.00037.
Kato, H., Onda, Y., Teramage, M., 2012. Depth distribution of 137Cs, 134Cs, and 131I in soil profile after Fukushima Dai-ichi nuclear power plant accident. J. Environ. Radioact. 111, 59–64. http://dx.doi.org/10.1016/j.jenvrad.2011.10.003.
Kinoshita, N., Sueki, K., Sasa, K., Kitagawa, J., Ikarashi, S., Nishimura, T., Wong, Y.-S., Satou, Y., Handa, K., Takahashi, T., Sato, M., Yamagata, T., 2011. Assessment of individual radionuclide distributions from the Fukushima nuclear accident covering central-east Japan. Proc. Natl. Acad. Sci. U. S. A. 108, 19526–19529. http://dx.doi.org/10.1073/pnas.1111724108.
Koarashi, J., Atarashi-Andoh, M., Matsunaga, T., Sato, T., Nagao, S., Nagai, H., 2012. Factors affecting vertical distribution of Fukushima accident-derived radiocesium in soil under different land-use conditions. Sci. Total Environ. 431, 392–401. http://dx.doi.org/10.1016/j.scitotenv.2012.05.041.
Kogure, T., Morimoto, K., Tamura, K., Sato, H., Yamagishi, A., 2012. XRD and HRTEM evidence for fixation of cesium ions in vermiculite clay. Chem. Lett. 41, 380–382. http://dx.doi.org/10.1246/cl.2012.380.
Kromek Group PLC, 2015. GR1 Spec Sheet; Revision 10 [WWW Document]. http://www.kromek.com/products_gr1spectrometer.asp (accessed 6.23.15).
Lepage, H., Evrard, O., Onda, Y., Lefèvre, I., Laceby, J.P., Ayrault, S., 2015. Depth distribution of cesium-137 in paddy fields across the Fukushima pollution plume in 2013. J. Environ. Radioact. 147, 157–164. http://dx.doi.org/10.1016/j.jenvrad.2015.05.003.
MacFarlane, J.W., Payton, O.D., Keatley, A.C., Scott, G.P.T., Pullin, H., Crane, R.A., Smilion, M., Popescu, I., Curlea, V., Scott, T.B., 2014. Lightweight aerial vehicles for monitoring, assessment and mapping of radiation anomalies. J. Environ. Radioact. 136, 127–130. http://dx.doi.org/10.1016/j.jenvrad.2014.05.008.
Malins, A., Okumura, M., Machida, M., Saito, K., 2015. Topographic effects on ambient dose equivalent rates from radiocesium fallout. In: M&C + SNA + MC 2015, p. 7.
Malins, A., Kurikami, H., Nakama, S., Saito, T., Okumura, M., Machida, M., Kitamura, A., 2016. Evaluation of ambient dose equivalent rates influenced by vertical and horizontal distribution of radioactive cesium in soil in Fukushima prefecture. J. Environ. Radioact. 151 (Pt 1), 38–49. http://dx.doi.org/10.1016/j.jenvrad.2015.09.014.
Martin, P.G., Payton, O.D., Fardoulis, J.S., Richards, D.A., Scott, T.B., 2015. The use of unmanned aerial systems for the mapping of legacy uranium mines. J. Environ. Radioact. 143, 135–140. http://dx.doi.org/10.1016/j.jenvrad.2015.02.004.
Martin, P.G., Payton, O.D., Fardoulis, J.S., Richards, D.A., Yamashiki, Y., Scott, T.B., 2016. Low altitude unmanned aerial vehicle for characterising remediation effectiveness following the FDNPP accident. J. Environ. Radioact. 151, 58–63. http://dx.doi.org/10.1016/j.jenvrad.2015.09.007.
Masson, O., Baeza, A., Bieringer, J., Brudecki, K., Bucci, S., Cappai, M., Carvalho, F.P., Connan, O., Cosma, C., Dalheimer, A., Didier, D., Depuydt, G., De Geer, L.E., De Vismes, A., Gini, L., Groppi, F., Gudnason, K., Gurriaran, R., Hainz, D., Halldórsson, Ó., Hammond, D., Hanley, O., Holeý, K., Homoki, Z., Ioannidou, A., Isajenko, K., Jankovic, M., Katzlberger, C., Kettunen, M., Kierepko, R., Kontro, R., Kwakman, P.J.M., Lecomte, M., Leon Vintro, L., Leppänen, A.-P., Lind, B., Lujaniene, G., Mc Ginnity, P., Mc Mahon, C., Malá, H., Manenti, S., Manolopoulou, M., Mattila, A., Mauring, A., Mietelski, J.W., Møller, B., Nielsen, S.P., Nikolic, J., Overwater, R.M.W., Pálsson, S.E., Papastefanou, C., Penev, I., Pham, M.K., Povinec, P.P., Ramebäck, H., Reis, M.C., Ringer, W., Rodriguez, A., Rulík, P., Saey, P.R.J., Samsonov, V., Schlosser, C., Sgorbati, G., Silobritiene, B.V., Söderström, C., Sogni, R., Solier, L., Sonck, M., Steinhauser, G., Steinkopff, T., Steinmann, P., Stoulos, S., Sýkora, I., Todorovic, D., Tooloutalaie, N., Tositti, L., Tschiersch, J., Ugron, A., Vagena, E., Vargas, A., Wershofen, H., Zhukova, O., 2011. Tracking of airborne radionuclides from the damaged Fukushima Dai-ichi nuclear reactors by European networks. Environ. Sci. Technol. 45, 7670–7677. http://dx.doi.org/10.1021/es2017158.
Merz, S., Steinhauser, G., Hamada, N., 2013. Anthropogenic radionuclides in Japanese food: environmental and legal implications. Environ. Sci. Technol. 47, 1248–1256. http://dx.doi.org/10.1021/es3037498.
METI, 2015. Areas to Which Evacuation Orders Have Been Issued [WWW Document]. http://www.meti.go.jp/english/earthquake/nuclear/roadmap/pdf/150905MapOfAreas.pdf (accessed 5.13.16).
MEXT, 2011. Results of the Airborne Monitoring by the Ministry of Education, Culture, Sports, Science and Technology and the U.S. Department of Energy, 6th May 2011.
MEXT, 2013. Results of the Sixth Airborne Monitoring and Airborne Monitoring Out of the 80km Zone of Fukushima Dai-ichi NPP.
MEXT, United States DoE, 2011. Results of Airborne Monitoring by the Ministry of Education, Culture, Sports, Science and Technology and the U.S. Department of Energy.
Miyahara, K., Tokizawa, T., Nakayama, S., 2012. Overview of the results of Fukushima decontamination pilot projects. In: IAEA International Experts' Meeting on Decommissioning and Remediation after a Nuclear Accident.
Mukai, H., Hirose, A., Motai, S., Kikuchi, R., Tanoi, K., Nakanishi, T.M., Yaita, T., Kogure, T., 2016. Cesium adsorption/desorption behavior of clay minerals considering actual contamination conditions in Fukushima. Sci. Rep. 6, 21543. http://dx.doi.org/10.1038/srep21543.
Nagao, S., Kanamori, M., Ochiai, S., 2013. Export of 134 Cs and 137 Cs in the Fukushima river systems at heavy rains by Typhoon Roke in September 2011. Biogeosciences. http://dx.doi.org/10.5194/bg-10-6215-2013.
NRA, 2011. Fukushima Prefecture Environmental Radiation Monitoring-mesh Investigation: Survey Meter (Ambient Dose Equivalent Rate).
Ohno, T., Muramatsu, Y., Miura, Y., Oda, K., Inagawa, N., Ogawa, H., Yamazaki, A., Toyama, C., Sato, M., 2012. Depth profiles of radioactive cesium and iodine released from the Fukushima Daiichi nuclear power plant in different agricultural fields and forests. Geochem. J. 46, 287–295. http://dx.doi.org/10.2343/geochemj.2.0204.
Qin, H., Yokoyama, Y., Fan, Q., Iwatani, H., Tanaka, K., Sakaguchi, A., Kanai, Y., Zhu, J., Onda, Y., Takahashi, Y., 2012. Investigation of cesium adsorption on soil and sediment samples from Fukushima prefecture by sequential extraction and EXAFS technique. Geochem. J. 46, 297–302. http://dx.doi.org/10.2343/geochemj.2.0214.
Sanada, Y., Kondo, A., Sugita, T., Torii, T., 2012. Distribution of radioactive cesium measured by aerial radiation monitoring. Hoshasen 38 (3), 137–140.
Sanada, Y., Kondo, A., Sugita, T., Nishizawa, Y., Youichi, Y., Kazutaka, I., Yasunori, S., Torii, T., 2014. Radiation monitoring using an unmanned helicopter in the evacuation zone around the Fukushima Daiichi nuclear power plant. Explor. Geophys.
Sawhney, B.L., 1972. Selective sorption and fixation of cations by clay minerals. A review. Clays Clay Min. 20, 93–100. http://dx.doi.org/10.1346/CCMN.1972.0200208.
Simons, M., Minson, S.E., Sladen, A., Ortega, F., Jiang, J., Owen, S.E., Meng, L., Ampuero, J.-P., Wei, S., Chu, R., Helmberger, D.V., Kanamori, H., Hetland, E., Moore, A.W., Webb, F.H., 2011. The 2011 magnitude 9.0 Tohoku-Oki earthquake: mosaicking the megathrust from seconds to centuries. Science 332, 1421–1425. http://dx.doi.org/10.1126/science.1206731.
Staunton, S., Dumat, C., Zsolnay, A., 2002. Possible role of organic matter in radiocaesium adsorption in soils. J. Environ. Radioact. 58, 163–173. http://dx.doi.org/10.1016/S0265-931X(01)00064-9.
Steinhauser, G., Brandl, A., Johnson, T.E., 2014. Comparison of the Chernobyl and Fukushima nuclear accidents: a review of the environmental impacts. Sci. Total Environ. 470–471, 800–817. http://dx.doi.org/10.1016/j.scitotenv.2013.10.029.
Stohl, A., Seibert, P., Wotawa, G., Arnold, D., Burkhart, J.F., Eckhardt, S., Tapia, C., Vargas, A., Yasunari, T.J., 2012. Xenon-133 and caesium-137 releases into the atmosphere from the Fukushima Dai-ichi nuclear power plant: determination of the source term, atmospheric dispersion, and deposition. Atmos. Chem. Phys. 12, 2313–2343. http://dx.doi.org/10.5194/acp-12-2313-2012.
Tagami, K., Uchida, S., Uchihori, Y., Ishii, N., Kitamura, H., Shirakawa, Y., 2011. Specific activity and activity ratios of radionuclides in soil collected about 20 km from the Fukushima Daiichi nuclear power plant: radionuclide release to the south and southwest. Sci. Total Environ. 409, 4885–4888. http://dx.doi.org/10.1016/j.scitotenv.2011.07.067.
Teramage, M.T., Onda, Y., Patin, J., Kato, H., Gomi, T., Nam, S., 2014. Vertical distribution of radiocesium in coniferous forest soil after the Fukushima nuclear power plant accident. J. Environ. Radioact. 137, 37–45. http://dx.doi.org/10.1016/j.jenvrad.2014.06.017.
Ueda, S., Hasegawa, H., Kakiuchi, H., Akata, N., Ohtsuka, Y., Hisamatsu, S., 2013. Fluvial discharges of radiocaesium from watersheds contaminated by the Fukushima Dai-ichi nuclear power plant accident. Jpn. J. Environ. Radioact. 118, 96–104. http://dx.doi.org/10.1016/j.jenvrad.2012.11.009.
Yamashiki, Y., Onda, Y., Smith, H.G., Blake, W.H., Wakahara, T., Igarashi, Y., Matsuura, Y., Yoshimura, K., 2014. Initial flux of sediment-associated radiocesium to the ocean from the largest river impacted by Fukushima Daiichi nuclear power plant. Sci. Rep. 4, 3714. http://dx.doi.org/10.1038/srep03714.
Yasunari, T.J., Stohl, A., Hayano, R.S., Burkhart, J.F., Eckhardt, S., Yasunari, T., 2011. Cesium-137 deposition and contamination of Japanese soils due to the Fukushima nuclear accident. Proc. Natl. Acad. Sci. U. S. A. 108, 19530–19534. http://dx.doi.org/10.1073/pnas.1112058108.
Yasutaka, T., Naito, W., 2015. Assessing cost and effectiveness of radiation decontamination in Fukushima Prefecture, Japan. J. Environ. Radioact. 151, 512–520. http://dx.doi.org/10.1016/j.jenvrad.2015.05.012.